INTERNATIONAL JOURNAL FOR NUMERICAL METHODS IN FLUIDS, VOL. 4, 441–457 (1984)

FINITE ELEMENT SIMULATION OF DIP COATING, I: NEWTONIAN FLUIDS

P. TANGUY*§, M. FORTIN† AND L. CHOPLIN*
Université Laval, Cité Universitaire Québec, Canada, G1K 7P4

SUMMARY

A finite element simulation of the dip coating process based on a discretization of the continuum with discontinuous pressure elements is presented. The algorithm computes the flow field from natural boundary conditions while an extra condition provided by the existence of free surface is employed to displace the meniscus location towards the actual position. The process is iterative and uses a pseudo-time stepping technique coupled to a cubic spline fitting of the free surface. Numerical predictions exhibit good agreement with experimental data for Newtonian fluids in the case of flat plate dip coating as well as in the case of wire dip coating.

KEY WORDS Finite Element Method Dip Coating Newtonian Fluid Free Surface

1. INTRODUCTION

This paper presents a simulation of a flow in which surface tension, viscosity and gravity play an important role. We consider the case when a web (flat plate or cylinder) is withdrawn vertically at a constant velocity from a liquid bath (Figure 1). During the process, a fluid layer is drawn along the moving web and a meniscus is formed at the interface between the air, the sheet and the liquid bath surface. The shape of the meniscus results from the equilibrium between viscous forces and surface tension forces. The operation described above is known as dip coating and is of considerable interest in many industries where it intervenes as a unit operation of more complex manufacturing processes.

From a practical point of view, the knowledge of the eventual coating thickness at the upper part of the meniscus and to a lesser extent the knowledge of the whole free surface location are required. They depend on the fluid properties as well as on the speed of withdrawal and can be predicted with a precise simulation of the flow.

Historically, the predictions of the free surface shape and of the eventual coating thickness were performed first assuming a Newtonian behaviour of the fluid. The first significant contribution was that of Landau and Levich[1] who derived from a simplification of the momentum equation, a differential equation for the thickness as a function of the height above the constant surface level. Since this pioneering work, the dip coating process has been extensively studied on both theoretical and experimental aspects, contributing thereby to improve Landau and Levich's approach. Because the majority of the fluids of interest for dip coating are essentially non-Newtonian in character, numerous attempts have been made in

* Department of Chemical Engineering
† Department of Mathematics
§ Present address: Dept. of Chem. Eng., TUNS, POB 1000, Halifax, NS, Canada, B3J 2X4

0271–2091/84/050441–17$01.70

Received September 1982
Revised February 1983

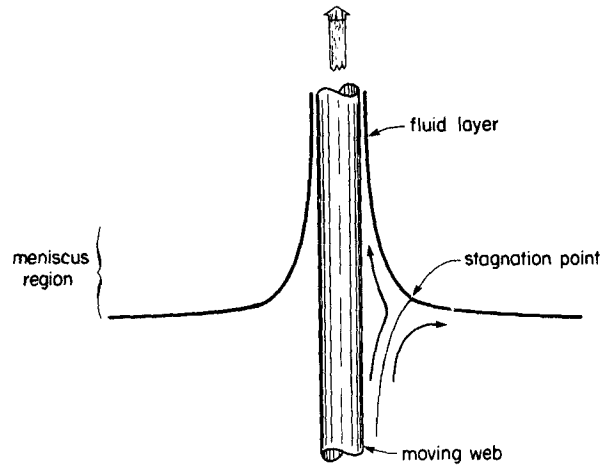

Figure 1. Dip coating process

order to adapt the Newtonian treatment to the non-Newtonian case. The rheological behaviour of these fluids is however quite complex and introduces additional non-linearities, resulting in very poor agreement with experiment. If we take into account the non-linearities inherent in the convective terms of the momentum equation and to the normal stress equilibrium condition on the free surface, the mathematical complexity of the problem becomes formidable.

That is the principal reason why most researchers have derived empirical correlations from experimental data and why little attention has been given to the purely numerical solution, except in the case of Newtonian fluids. Interesting reviews have been written by Middleman[2] and Higgins *et al.*[3]

Finite difference methods were used by Lee and Tallmadge[4] and Marques *et al.*[5] They used stream function–vorticity implicit schemes, which are very difficult to adapt to complex non-Newtonian behaviour. This is not the case for the Eulerian formulation with the finite element method. Moreover finite element methods are more convenient to fit irregular boundaries, as, for example, free surfaces.

In the present work, we used the finite element method to model the dip coating process for Newtonian and non-Newtonian fluids. Part I describes the finite element approximation and the method used for the computation of the free boundary. Numerical results for Newtonian flows are presented and compared with experimental data. Part II will deal with non-Newtonian fluids and present a widely applicable algorithm for the solution of such flows.

2. PROBLEM, DEFINITIONS AND NOTATIONS

We consider the equations of viscous incompressible flow:

$$\rho(\dot{\mathbf{u}}+\mathbf{u}\cdot\nabla\mathbf{u})+\nabla\cdot\boldsymbol{\tau}=\rho\mathbf{f} \tag{1a}$$

$$\nabla\cdot\mathbf{u}=0 \tag{1b}$$

Here $\mathbf{u}$ denotes the velocity of the fluid, ρ its density and $\boldsymbol{\tau}$ the stress tensor. The body force $\mathbf{f}$ is, in practice, of the form $\mathbf{f}=\{0, g\}$, where g is the gravitational acceleration constant. This study will be restricted to bidimensional or axisymmetric flows, in which $\mathbf{u}$ has only two components. We shall also consider steady flows in which $\dot{\mathbf{u}}=\partial\mathbf{u}/\partial t=0$.

The stress tensor $\boldsymbol{\tau}$ is written as

$$\boldsymbol{\tau} = \boldsymbol{\tau}^{\mathrm{D}} + p\boldsymbol{\delta}; \qquad \sum_i \tau_{ii}^{\mathrm{D}} = 0 \tag{2a}$$

Classically, the deviatoric $\boldsymbol{\tau}^{\mathrm{D}}$ is related through a *constitutive equation* to the rate-of-strain tensor $\dot{\boldsymbol{\gamma}}(\mathbf{u})$, that is:

$$\boldsymbol{\tau}^{\mathrm{D}} = \varphi(\dot{\boldsymbol{\gamma}}(\mathbf{u})) \tag{2b}$$

For the dip coating process, the tensor $\dot{\boldsymbol{\gamma}}$ can be written in Cartesian co-ordinates (x, y) as follows:

$$\dot{\boldsymbol{\gamma}} = \begin{bmatrix} \dfrac{\partial u}{\partial x} & 0 & \dfrac{1}{2}\left(\dfrac{\partial u}{\partial y} + \dfrac{\partial v}{\partial x}\right) \\ 0 & 0 & 0 \\ \dfrac{1}{2}\left(\dfrac{\partial u}{\partial y} + \dfrac{\partial v}{\partial x}\right) & 0 & \dfrac{\partial v}{\partial y} \end{bmatrix} \tag{2c}$$

and in axisymmetrical co-ordinates:

$$\dot{\boldsymbol{\gamma}} = \begin{bmatrix} \dfrac{\partial u}{\partial r} & 0 & \dfrac{1}{2}\left(\dfrac{\partial u}{\partial z} + \dfrac{\partial v}{\partial r}\right) \\ 0 & \dfrac{u}{r} & 0 \\ \dfrac{1}{2}\left(\dfrac{\partial u}{\partial z} + \dfrac{\partial v}{\partial r}\right) & 0 & \dfrac{\partial v}{\partial z} \end{bmatrix} \tag{2d}$$

In equations (2c) and (2d), u and v denote, respectively, the components of the vector $\mathbf{u}$ in the x (or r) and y (or z) directions.

We shall, as mentioned previously, restrict the present part to the Newtonian case, for which:

$$\boldsymbol{\tau}^{\mathrm{D}} = 2\mu\dot{\boldsymbol{\gamma}}(\mathbf{u}) \tag{2e}$$

Here, μ denotes the viscosity of the fluid.

A complete definition of the problem requires boundary conditions; they are of Dirichlet's type on the known parts of the boundary (Figure 2). On the free boundary Γ_{F}, let $\mathbf{n}$ be the outward oriented normal and $\mathbf{t}$ the tangential vector as shown by Figure 3. Let us define on Γ_{F} the normal and tangential stress components:

$$\tau_{nn} = \sum_{i,j} \tau_{ij} n_i n_j; \qquad \tau_{nt} = \sum_{i,j} \tau_{ij} n_i t_j \tag{3a}$$

We must then have on Γ_{F},

$$\tau_{nn} = \frac{\sigma}{R_1} - p_0, \qquad \text{for plane flows} \tag{3b}$$

$$\tau_{nn} = \frac{\sigma}{R_1} - \frac{\sigma}{R_2} - p_0, \quad \text{for axisymmetric flows} \tag{3c}$$

$$\tau_{nt} = \mu\left[\frac{\partial u_t}{\partial n} + \frac{\partial u_n}{\partial t}\right] = 0 \tag{3d}$$

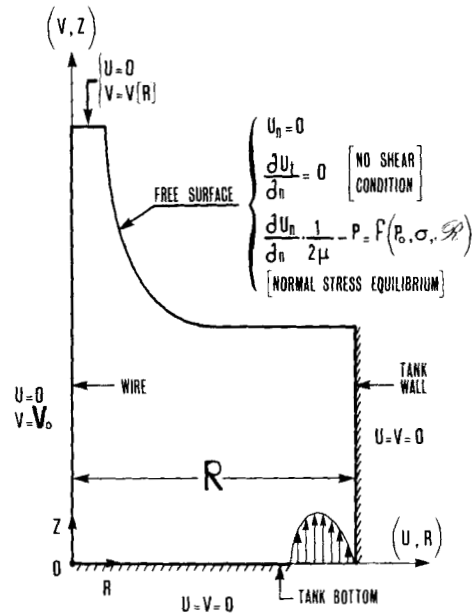

Figure 2. Boundary conditions for wire dip coating (at equilibrium)

Conditions (3b) and (3a), where σ represents the surface tension of the fluid, R_1 and R_2 the radii of curvature and p_0 the atmospheric pressure, express the equilibrium of viscous forces with surface tension forces. In the axisymmetric case (see Figure 3) we must take into account two radii of curvature with opposite effects, whereas in the other case considered here, only one radius of curvature intervenes.

On the free surface, we must also have,

$$u_n = \mathbf{u} \cdot \mathbf{n} = 0 \tag{4}$$

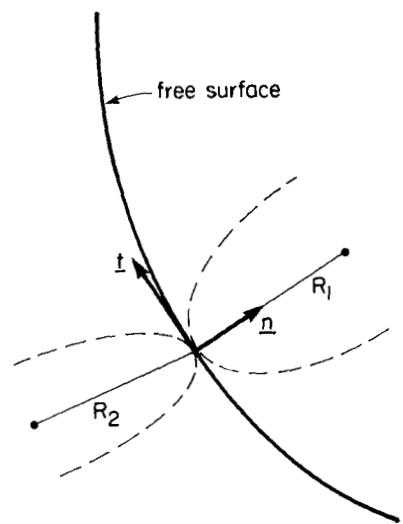

Figure 3. Free surface coordinate system

which expresses that the flow is tangential to Γ_F. If the free boundary Γ_F were known, either (3b) and (3a) or (3b) and (4) would be consistent sets of boundary conditions. The third condition must be used to locate Γ_F. We first consider the case of a *fixed known boundary* Γ_F.

To give a variational formulation to this problem, we define [6]:

$$a(\mathbf{u}, \mathbf{v}) = 2\mu \int_\Omega \dot{\gamma}(\mathbf{u}) : \dot{\gamma}(\mathbf{v})\, dx = 2\mu \int_\Omega \sum_{i,j} \dot{\gamma}_{ij}(\mathbf{u}) \dot{\gamma}_{ij}(\mathbf{v})\, dx \tag{5a}$$

$$b(\mathbf{u}, \mathbf{u}, \mathbf{v}) = \int_\Omega (\mathbf{u} \cdot \nabla \mathbf{u}) \cdot \mathbf{v}\, dx \tag{5b}$$

$$c(p, \mathbf{v}) = \int_\Omega p \nabla \cdot \mathbf{v}\, dx \tag{5c}$$

We now consider Ω being known, the weak problem written for the plane flow case for simplicity:

$$a(\mathbf{u}, \delta\mathbf{u}) + b(\mathbf{u}, \mathbf{u}, \delta\mathbf{u}) - c(p, \delta\mathbf{u}) = \int_\Omega \mathbf{f} \cdot \delta\mathbf{u}\, dx + \int_{\Gamma_F} \left(\frac{\sigma}{R_1} - p_0\right) \delta\mathbf{u} \cdot \mathbf{n}\, d\Gamma_F, \qquad \forall \delta\mathbf{u} \in \mathcal{V} \tag{6a}$$

$$c(\delta p, \mathbf{u}) = 0, \qquad \forall \delta p \in \mathcal{Q} \tag{6b}$$

The spaces $\mathcal{V}$ and $\mathcal{Q}$ are the spaces of test velocities and test pressure respectively. The test functions of $\mathcal{V}$ vanish on the boundaries where Dirichlet's conditions are imposed.

Integrating (5a) by parts and using the result in (6a) shows that boundary conditions (3b) and (3d) (or (3c) and (3d) in the axisymmetric case) are *natural boundary conditions* in this formulation.

Remark 1

The natural boundary conditions would not be the same if $\int_\Omega \nabla\mathbf{u} : \nabla\mathbf{v}\, dx$ has been used instead of $a(\mathbf{u}, \mathbf{v})$ to represent the viscous terms in the equations. Even if this form is equivalent in the case of Dirichlet's boundary conditions, it does not yield, when integrated by parts, the same natural boundary conditions. Using the correct expression is very important for free surface problems if one wants to obtain the stress balance condition.

Remark 2

If we neglect the inertial terms $\mathbf{u} \cdot \nabla\mathbf{u}$, (6a) and (6b) is equivalent to a saddle point problem:

$$\inf_{\mathbf{v} \in \mathcal{V}} \sup_{p \in \mathcal{Q}} \left\{ \frac{\mu}{\rho} \int_\Omega |\dot{\gamma}(\mathbf{v})|^2\, dx - \int_\Omega p \nabla \cdot \mathbf{v}\, dx - \int_\Omega \mathbf{f} \cdot \mathbf{v}\, dx - \int_{\Gamma_F} \left(\frac{\sigma}{R_1} - p_0\right) \mathbf{v} \cdot \mathbf{n}\, d\Gamma_F \right\} \tag{7}$$

We thus have a mixed formulation of our problem and this point will have implications on the choice of the discretization.

3. FINITE ELEMENT APPROXIMATION

3.1. *Description of the method*

It is well known that the approximation of incompressible materials by finite elements requires special care, and that one has to satisfy the celebrated Brezzi–Babuska condition[7]

between the approximations of velocity and pressure. In the past the biquadratic velocity–bilinear (continuous) pressure element, denoted Q_{94}, has been widely used in numerous bidimensional flow problems. The present state-of-the-art however clearly implies, in our view, that the biquadratic velocity–linear (discontinuous) pressure element, which we denote Q_{93}, is the best choice of a quadrilateral element.[8,9]

This element is, moreover, compatible with the enriched-quadratic velocity–linear pressure triangular element, denoted T_{73}, of Crouzeix and Raviart.[10] This element is nothing but the standard quadratic triangular element to which a bubble function ($\lambda_1\lambda_2\lambda_3$ in barycentric co-ordinates) has been added for the sake of satisfying the compatibility condition. The degrees of freedom of these elements are presented on Figure 4.

Simultaneous use of quadrilaterals and triangles allows more flexibility in mesh generation (see Figures 5(a) and 5(b)). It can be shown that both elements provide a second-order approximation of the equations of change at least in ideal cases. Using a discontinuous linear pressure means that on each element, the divergence-free condition is approximated by a set of three linear constraints. In our program, pressure has been defined by an expression of the form $(a_0 + b_0\xi_1 + c_0\xi_2)$ on a *reference* element. The constant term is the value of the pressure at the barycentre whereas the two extra terms have no direct sense on the current element, even if they can be used to compute pressure values at any point.

Denoting the vector of nodal values of $\mathbf{u}$ by $\mathbf{U}$ and the nodal pressures (as defined above) by p, we have from (6a) and (6b) a set of non-linear equations to solve. Setting:

$$\langle A\mathbf{U}, \mathbf{V}\rangle = a(\mathbf{u}, \mathbf{v}) \tag{8a}$$

$$\langle B(\mathbf{U})\mathbf{U}, \mathbf{V}\rangle = b(\mathbf{u}, \mathbf{u}, \mathbf{v}) \tag{8b}$$

$$\langle C\mathbf{U}, P\rangle = c(\mathbf{u}, p) \tag{8c}$$

$$\langle \mathbf{F}, \mathbf{V}\rangle = \int_\Omega \mathbf{f}\cdot\mathbf{v}\,dx - \int_{\Gamma_F} \left(\frac{\sigma}{R_1} - p_0\right)\mathbf{v}\cdot\mathbf{n}\,d\Gamma_F, \tag{8d}$$

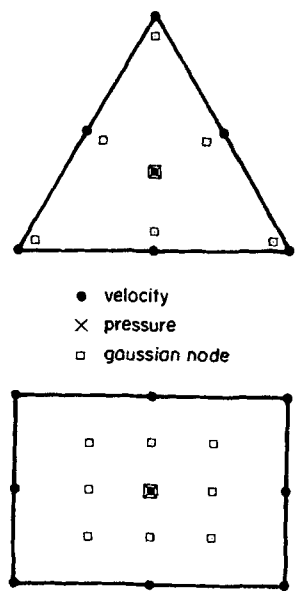

Figure 4. Elements T_{73} and Q_{93}

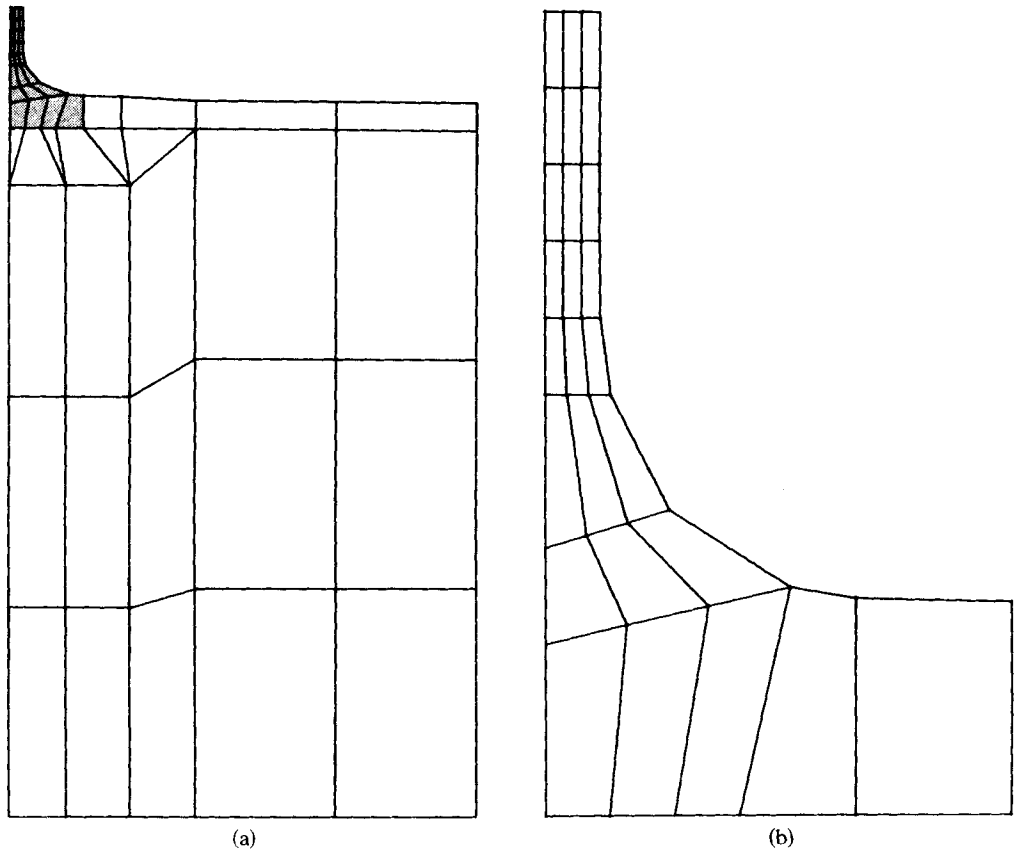

Figure 5. (a) Finite element mesh for dip coating. (b) Details of finite element mesh in the meniscus region

we obtain

$$A\mathbf{U}+B(\mathbf{U})\mathbf{U}+C^{\mathrm{T}}P=\mathbf{F} \tag{9a}$$

$$C\mathbf{U}=0 \tag{9b}$$

The matrix C can be decomposed into (18×3) (for quadrilaterals) or (14×3) (for triangles) matrices on each element.

To solve this discrete system, we use an *exact* penalty method in the sense of Engelman *et al.*[8] (see also Bercovier and Engelman,[11] Fortin[9]). The penalty method is completely compatible with the Q_{93} element in the sense of Malkus and Hughes[12] We set:

$$P=\frac{1}{\lambda}S^{-1}C\mathbf{U} \tag{10}$$

where S is any non-singular matrix and λ the parameter of penalization. In practice, we used the identity matrix weighted by the area of the element in order to get a good scaling. We thus obtain:

$$A\mathbf{U}_\lambda+B(\mathbf{U}_\lambda)\mathbf{U}_\lambda+\frac{1}{\lambda}C^{\mathrm{T}}S^{-1}C\mathbf{U}_\lambda=\mathbf{F} \tag{11}$$

This non-linear system can be solved by Newton's method but this requires factoring (and

assembling) a new matrix at each iteration. In the problem we consider which involves very viscous fluids, inertial terms can often be neglected and the problem then becomes linear.

The error introduced by penalization can be completely removed using a very simple iterative scheme (for a complete justification, see Reference 13). The idea is to write (10) as an *updating* of the pressure:

$$P^{n+1} = P^n + \frac{1}{\lambda} S^{-1} C\mathbf{U}^{n+1} \tag{12}$$

along with

$$A\mathbf{U}_\lambda^{n+1} + B(\mathbf{U}_\lambda^{n+1})\mathbf{U}_\lambda^{n+1} + C^{\mathrm{T}}P^n + \frac{1}{\lambda} C^{\mathrm{T}}S^{-1}C\mathbf{U}_\lambda^{n+1} = \mathbf{F} \tag{13}$$

This process is shown to converge by Fortin and Glowinski.[14] In fact, it does so in one iteration if λ is small enough. In cases where a too small value could cause conditioning problems, the iterative process ensures accurate values in all cases. This is a very simple example of mixing penalty and duality technique, an idea that will be basic to our treatment of non-Newtonian fluid flows.

3.2. *Numerical test*

Before presenting the computation of free boundaries and results on the dip coating problem, we would like to present a comparison we made between the Q_{93} and Q_{94} elements. Even if the real significance of this test is somewhat limited, we consider it may be worth being presented rapidly.

The test is on a recirculating flow inside an annulus, as shown in Figure 6. This can be seen as the popular driven cavity problem with axisymmetric co-ordinates and has been chosen because of its similarities with the dip coating process. If the annulus is very long, an analytical solution[15] for the velocity profile can be derived, neglecting end effects:

$$V = V_0 \left\{ \frac{(1-\xi^2)\left[1 + \dfrac{2k^2}{1-k^2} \ln k\right] + (1-k^2)\ln \xi}{1-k^2+(1+k^2)\ln k} \right\} \tag{14}$$

where

$$\xi = \frac{r}{R} \qquad \text{and} \qquad k = \frac{r_0}{R}.$$

This is of course in fact a linear solution. In the numerical test we used a length–radius ratio of 10 in order to eliminate end effects. The grid and boundary conditions are shown in Figure 7. The results are presented in Figure 8 and Table I. Both computations show a good agreement with the analytical profile. The Q_{93} element however shows a more regular distribution of errors and better results for the larger values of the velocity.

4. DIP COATING SIMULATION

4.1. *The free boundary problem*

Finding the shape of the free meniscus is an essential part of the dip coating problem. Although other approaches are possible,[16] the classical way of finding a free surface is to use, on some initial estimate of the surface, a set of consistent boundary conditions, to compute a flow using these conditions and to update the surface using the extra boundary condition.

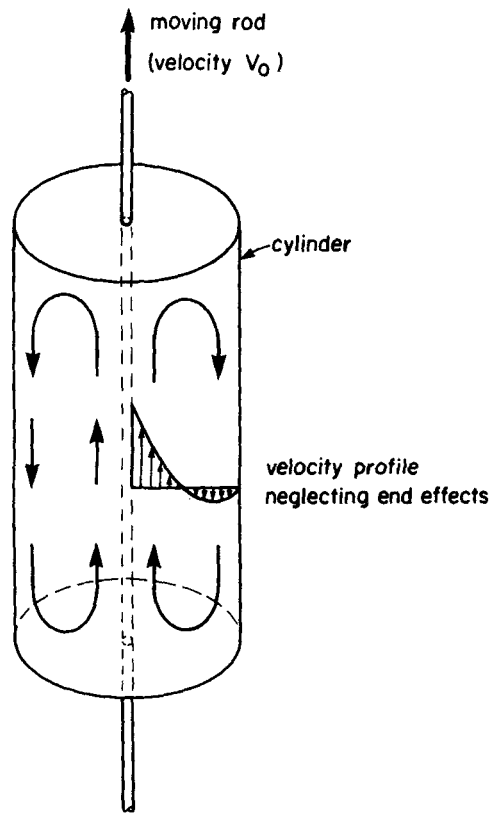

Figure 6. Recirculating flow into an annulus

Many possibilities exist to devise such a procedure. We chose to solve problems involving the natural boundary conditions ((3b) or (3c) and (3d)) for the computation of the flow. The reason was that these conditions require no special treatment and are included in the variational formulation. Moreover it is easy to check if the last condition, $\mathbf{u} \cdot \mathbf{n} = 0$ on Γ_F, is satisfied while checking directly (3b) for instance, requires the stress values on Γ_F. These values are not readily available, with sufficient precision, in the discretization we used.

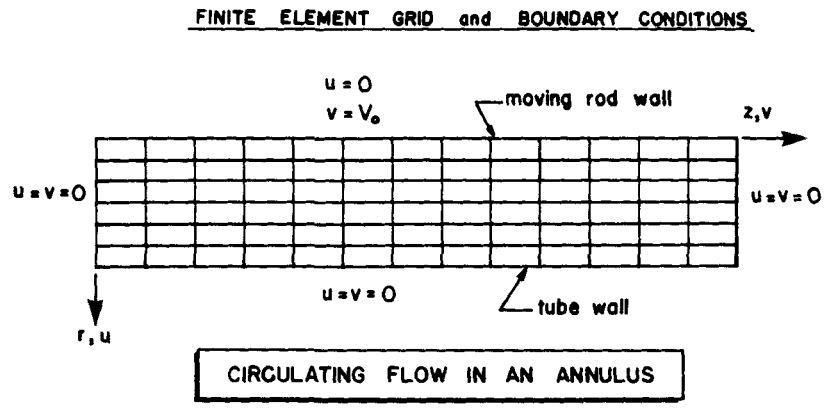

Figure 7. Grid and boundary conditions for recirculating flow

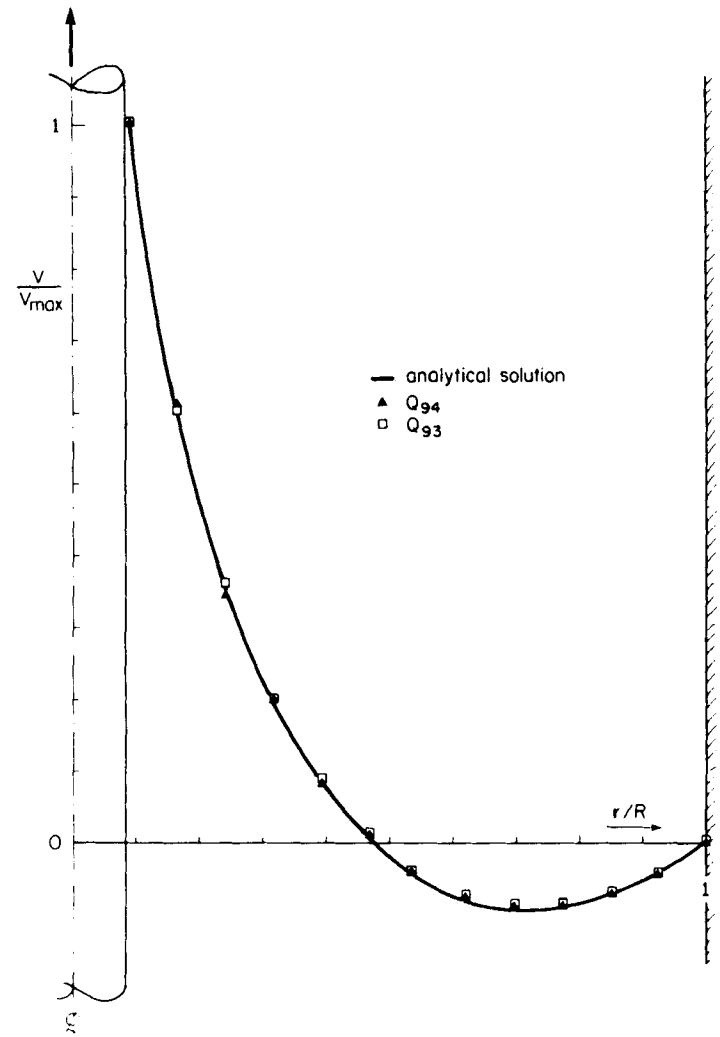

Figure 8. Velocity profiles in the annulus, far from the edges: comparison between numerical and analytical solutions

Even this choice of boundary conditions does not lead to a unique updating procedure for the free boundary. A standard procedure[17,18] is to compute a new boundary by solving a discrete version of the differential equation for $(x, y) \in \Gamma_F$:

$$\frac{dy}{dx} = \frac{v}{u}, \qquad y(x_0) = y_0 \tag{15}$$

where (x_0, y_0) is some known point of the boundary.

Equation (15) expresses that Γ_F should be parallel to the flow. This method seems to work properly for free-jet flows but cannot be applied in our case for which a stagnation point exists on the free surface. One would then have to integrate (15) through a singular point.

Table I. Velocity profile for a recirculating flow into an annulus: comparison between numerical predictions with Q_{94} and Q_{93} elements and analytical solution

r/R	V/V_0 analytical	V/V_0 Q_{94} element	V/V_0 Q_{93} element
0·091	1	1	1
0·16675	0·59167	0·60796 (+0·01629)	0·59823 (+0·00654)
0·2425	0·35193	0·34489 (−0·00704)	0·35842 (+0·00649)
0·31825	0·19136	0·20248 (+0·01112)	0·19914 (+0·00778)
0·394	0·07912	0·08233 (+0·00321)	0·08663 (+0·00751)
0·46975	0·00081	0·00888 (+0·00807)	0·00790 (+0·00709)
0·50455	−0·05142	−0·04569 (+0·00573)	−0·04470 (+0·00672)
0·62125	−0·08238	−0·07594 (+0·00644)	−0·07613 (+0·00625)
0·697	−0·09518	−0·09006 (+0·00512)	−0·08979 (+0·00539)
0·77275	−0·09197	−0·08762 (+0·00435)	−0·08767 (+0·00430)
0·8485	−0·07432	−0·07122 (+0·00310)	−0·07128 (+0·00304)
0·92425	−0·04337	−0·04178 (+0·00159)	−0·04176 (+0·00161)
1	0	0	0

4.2. Description of the method

We used a method that seems less classical even if it is suggested by Zienkiewicz and Godbole.[19] It is an imitation of the actual movement of the free surface in a time-dependent computation. We say that we make pseudo-time stepping. Let $\mathbf{x}^k$ be a point of Γ_F at step k and $\mathbf{u}.\mathbf{n}$ the value of the normal velocity at this point. We set:

$$\mathbf{x}^{k+1} = \mathbf{x}^k + \alpha(\mathbf{u}.\mathbf{n})\mathbf{n} \tag{16}$$

where α is a dummy time step. We thus move the point normally to Γ_F at a distance proportional to $\mathbf{u}.\mathbf{n}$. Choosing the value of α will be discussed below. In practice only the vertices of the elements were moved by (16). A cubic spline is first fitted to the points to be moved. This enables us to compute a good value of the normal $\mathbf{n}$ (it also provides a convenient way of computing curvature). The vertices are then moved according to (16) and a new spline is used to compute the midpoints of the element sides which we need to recompute the flow. The boundary of the higher element (cf. Figure 9) was considered vertical and was moved in unison with the last point of the spline.

Remark 3

The spline was parameterized by the arc length s of the piecewise linear fit to the same points. We thus get two cubic splines $x(s)$, $y(s)$. This arc length s is close enough to the exact arc length to ensure that the fitted spline was almost of minimum quadrature in the usual sense of cubic splines. We also tried using a quadratic spline that seemed more adapted to our isoparametric element. This proved much less stable in practical computation and was discarded.

The boundary conditions of the outgoing flow were computed assuming a pure shear flow. This implies that our mesh must extend high enough to make this assumption realistic. We

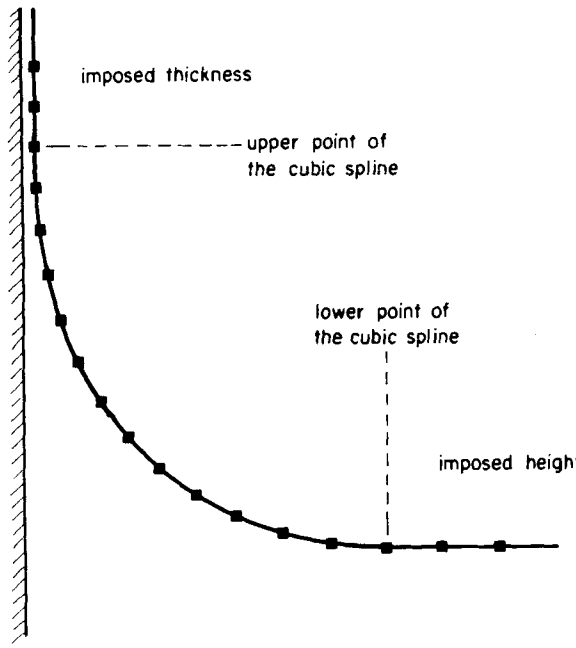

Figure 9. Cubic spline fitting of the free surface shape

thus have, h denoting the thickness,

$$V_{out} = V_0 + \frac{g}{4}(r^2 - r_0^2) - g\frac{h^2}{2}\ln\left(\frac{r}{r_0}\right) \tag{17a}$$

in the axisymmetric case or

$$V_{out} = V_0 + \frac{g}{2}x^2 - ghx, \tag{17b}$$

in the case of plane flow.

At each step, a new value of h is computed as described above. The inflow V_{in} is adjusted in order to match (17a) or (17b) so that the total mass be conserved.

Remark 4

In the pure shear flow, one has:

$$p = p_0 + \frac{\sigma}{R_2} \quad \text{(see Figure 3)} \tag{18}$$

Thus for a plane flow we have $p = p_0$ whereas for an axisymmetric flow we have $p > p_0$.

The determination of a good value for α in (16) was done experimentally first. It is also possible to use a criterion for the choice of α.

For a given boundary Γ_F, and the associated flow, let us define:

$$J(\Gamma_F) = \int_{\Gamma_F} (\mathbf{u} \cdot \mathbf{n})^2 \, ds \tag{19}$$

Minimizing $J(\Gamma_F)$ is equivalent to solving our problem.[20] Given an initial choice α_0 of α, we

recompute $J(\Gamma_F)$ by moving the boundary by α and $2\alpha_0$ from the same initial position. We thus obtain three points ($\alpha = 0$, α_0 and $2\alpha_0$) and a parabolic fit gives us the best local value of α.

4.3. *Results and discussion*

We have calculated the free surface shape and the eventual thickness for Newtonian fluids in three cases.

The first case corresponds to flat plate coating, whereas the others correspond to wire coating. In order to compare the numerical calculation to experimental results, we have taken from the literature[21] data for flat plate coating and for the wire coating, and we have designed an experimental device whose description can be found elsewhere, together with experimental procedure.[22]

For all cases, the physical properties of the fluids used and the dimensionless groups corresponding to the dynamic of the dip coating process are presented in Tables II and III. Figures 10–12 show the comparison between the experimental meniscus profile, and that obtained by numerical calculations.

In Table IV, we present the numerically predicted eventual thickness value as compared with the measured thickness. In all cases, the agreement is fairly good.

The number of iterations necessary to obtain a stable free surface location strongly depends on the quality of the initial guess, particularly its shape. We have shown in Figures 10 and 11 its location with respect to the numerical and experimental results. With these initial guesses, computations never required more than 15 free surface iterations. The criterion of convergence we used for the determination of this free surface is defined by comparing the magnitude of the normal velocity, u_n, at the free surface nodes to the withdrawal velocity, V_0, by:

$$\max_{x_i} \left[\frac{u_n(x_i)}{V_0} \right] < \varepsilon \tag{20}$$

which is equivalent by (16) to a classical convergence criterion on the nodes displacement.

Table II. Physical properties of the fluids at 25°C and atmospheric pressure

	μ[=]Pa . s	ρ[=]kg/m^3	σ[=]N/m.
Lee and Tallmadge[21]	1·31	885	0·0327
Vitrea oil	2·9	910	0·0359

Table III. Dimensionless groups for dip coating experiments

	$Re = \frac{h_{exp} V_0 \rho}{\mu}$	$Ca = \mu \frac{V_0}{\sigma}$	
Lee and Tallmadge[21] (V_0 = 3·31 cm/s)	0·032	1·33	Flat plate coating
Vitrea oil (V_0 = 2.41 cm/s)	0·0094	1·95	Wire coating
Vitrea oil (V_0 = 7·47 cm/s)	0·045	6·03	

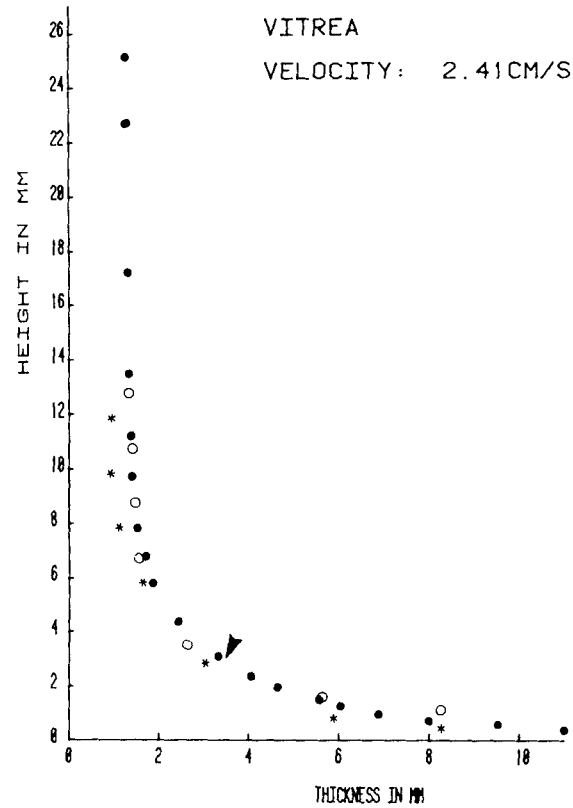

Figure 10. Wire meniscus profile for vitrea oil at $V_0 = 2{\cdot}41$ cm/s: * initial guess; ○ numerical prediction; ● experimental measurement

In Figure 13, a typical flow field is presented; it corresponds to the wire dip coating case ($V_0 = 2{\cdot}41$ cm/s). This result shows no surprising feature and can be compared with those of Lee and Tallmadge.[21] The observation of the flow lines clearly shows the existence of a stagnation point on the free surface. This point delimits two areas in which the fluid flows in opposite directions. The prediction of the location of the stagnation point by our finite element algorithm agrees with previous results. Such a point is located approximately at a meniscus thickness equal to 2·5 times the eventual coating thickness (see the arrows in Figures 10–12).

Another result of interest is that observed on the free surface between the initial guess and the final location. The displacement of the free surface between two consecutive iterations shows a propagation of a swell (Figure 14), from the free surface constant level to the upper part of the meniscus. This phenomenon is similar to that observed when the web is suddenly accelerated and is due to the time-stepping technique which simulates a time-dependent situation.

Finally, we have tested the influence of the inertial terms of the equation of motion on the computed results. We have noticed that these convective terms do not significantly influence the prediction of the eventual coating thickness in the upper part of the meniscus; nevertheless, the eventual shape of the lower part of the meniscus is affected and appears to be more narrow, in contradiction to experimental results.

If the interest is to predict the eventual thickness only, this omission will be very useful

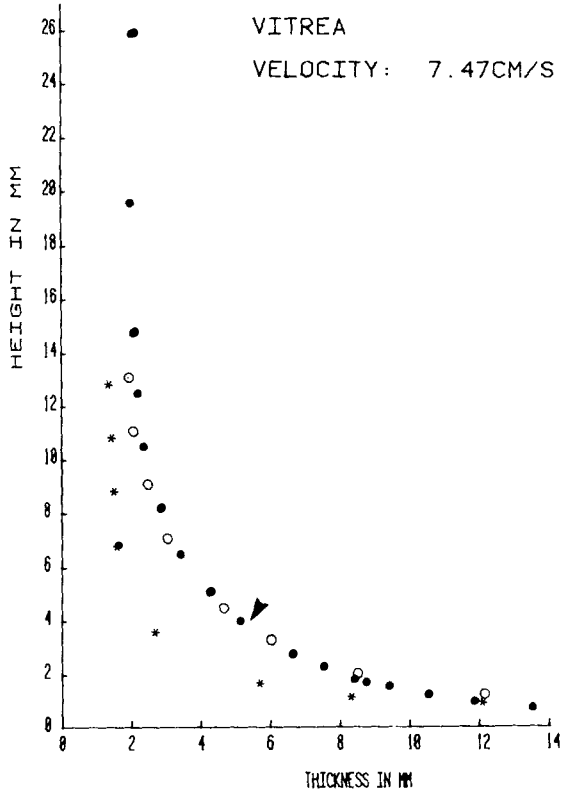

Figure 11. Wire meniscus profile for vitrea oil at $V_0 =$ 7·47 cm/s: the symbols are the same as in Figure 10

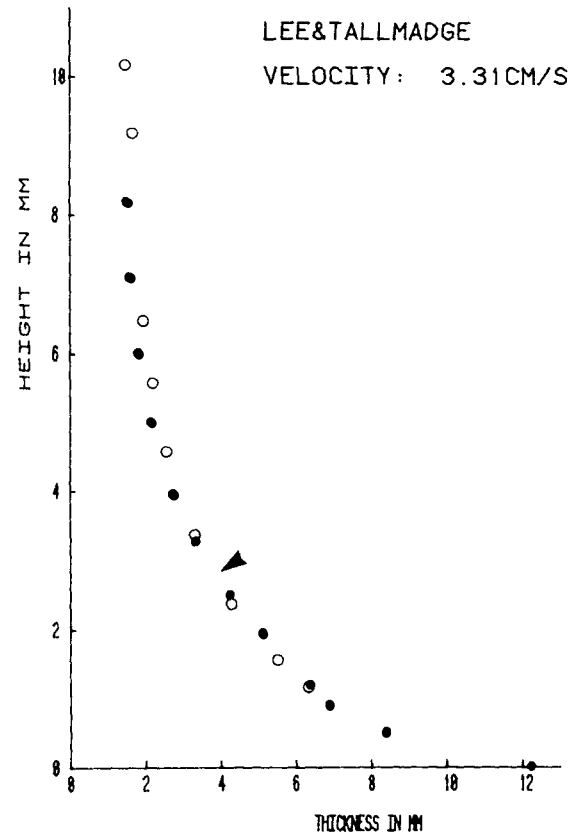

Figure 12. Flat plate meniscus profile at $V_0 = 3{\cdot}31$ cm/s: ● experimental data (Lee and Tallmadge[21]); ○ numerical prediction

because it is possible to save up to 50 per cent of the CPU time by this artificial means. For the three cases studied (the mesh contained 233 nodes and 50 elements), the mean CPU time was about 5 minutes on a 4341 IBM unit.

5. CONCLUSIONS

We have shown in this first part that the dip coating process can be successfully simulated by Galerkin method coupled to a discontinuous pressure element discretization of the con-

Table IV. Comparison between numerically predicted eventual thickness and experimental valve

	$h[=]$mm numerical	$h[=]$mm experimental	
Lee and Tallmadge[21] ($V_0 = 3{\cdot}31$ cm/s)	1·43	1·43	Flat plate coating
Vitrea oil ($V_0 = 2{\cdot}41$ cm/s)	1·28	1·24	Wire coating
Vitrea oil ($V_0 = 7{\cdot}47$ cm/s)	1·85	1·93	

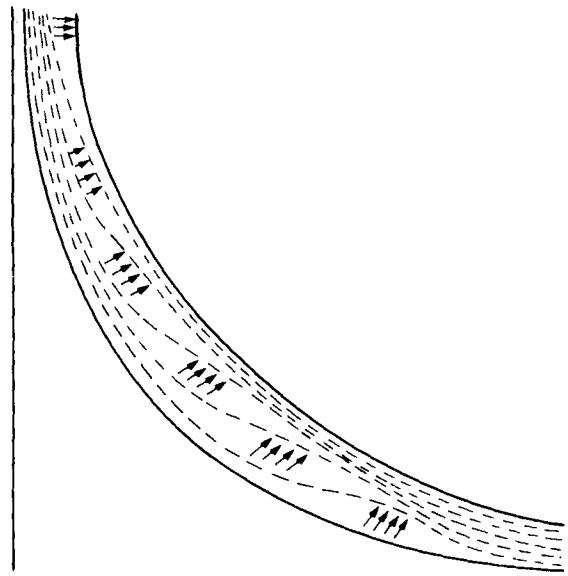

Figure 13. Typical propagation of a free surface swell during the iterative process

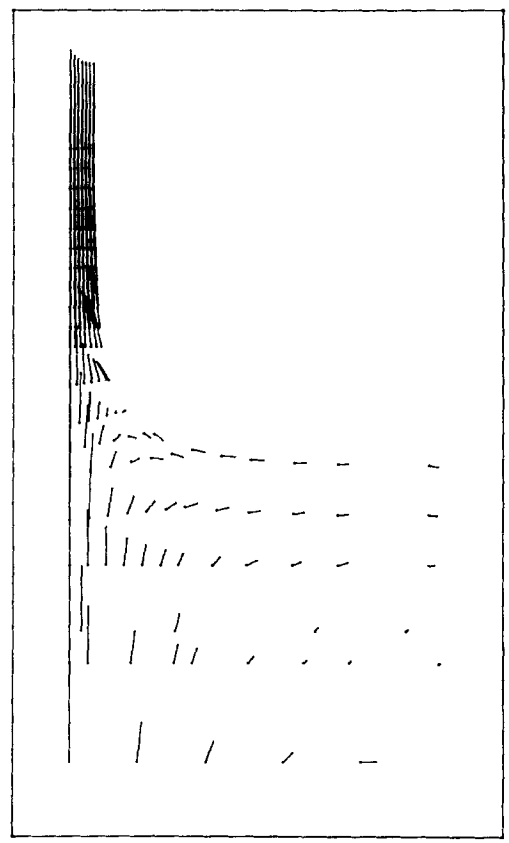

Figure 14. Velocity field in the meniscus region in the case of Figure 10

tinuum. This method enables us to correctly predict the complex axisymmetric flow situation which involves a free surface and a stagnation point.

Agreement of our numerical predictions with already published results and with direct measurements is noteworthy in Newtonian case.

The second part of this work will deal with non-Newtonian modelling of this dip coating process, with peculiar attention to the treatment of non-linearities introduced by complex rheological behaviour.

ACKNOWLEDGEMENTS

The authors acknowledge the financial assistance provided by the NSERC of Canada.

REFERENCES

1. L. Landau and B. Levich, 'Dragging of a liquid by a moving plate', *Acta Physicochimica (USSR)*, **17,** 41 (1942).
2. S. Middleman, in *Fundamentals of Polymer Processing*, McGraw Hill, 1977.
3. B. G. Higgins, W. J. Silliman, R. A. Brown and L. E. Scriven, 'Theory of meniscus shape in film flows. A synthesis', *Ind. Eng. Chem., Fundam.*, **16,** 393 (1977).
4. C. Y. Lee and J. A. Tallmadge, 'Dynamic meniscus profiles in free coating III. Predictions based on two-dimensional flow fields', *AIChE J.*, **20,** 1079 (1974).
5. D. Marques, V. Costanza and R. L. Cerro, 'Dip coating at large capillary numbers: an initial value problem', *Chem. Eng. Sci.*, **33,** 87 (1978).
6. R. Teman, in *Navier–Stokes Equations*, North Holland, Amsterdam, 1979.
7. F. Brezzi, 'On the existence uniqueness and approximation of saddle-point problems arising from Lagrangian multipliers', *RAIRO Série Analyse Numérique*, **8,** 129 (1974).
8. M. S. Engelman, R. L. Sani, P. M. Gresho and M. Bercovier, 'Consistent vs. reduced integration penalty methods for incompressible media using several old and new elements', *Int. J. Numer. Methods Fluids*, **2,** 25 (1982).
9. M. Fortin, 'Two comments on "Consistent vs. reduced integration penalty methods for incompressible media using several old and new elements" by M. S. Engelman *et al.*', *Int. j. numer. methods fluids*, **2,** 93 (1983).
10. M. Crouzeix and P. A. Raviart, 'Conforming and non-conforming finite element methods for solving the stationary Stokes equations', *RAIRO Série Analyse Numérique*, **7,** 33 (1973).
11. M. Bercovier and M. Engelman, 'A finite element for the numerical solution of viscous incompressible flows', *J. Comp. Physics*, **30,** 181 (1979).
12. D. S. Malkus and T. J. R. Hughes, 'Mixed finite element methods, reduced and selective integration techniques: a unification of concepts', *Comp. Meth. Appl. Mech. Eng.*, **15,** 63 (1978).
13. M. Fortin and F. Thomasset, 'Mixed finite element methods for incompressible flow problems', *J. Comp. Physics*, **31,** 113 (1979).
14. M. Fortin and R. Glowinski, *Résolution Numérique de Problèmes aux Limites par des Méthodes de Lagrangien Augmenté*, Dunod, 1982.
15. R. B. Bird, R. C. Armstrong and O. Hassager, in *Dynamics of Polymeric Liquids, Vol. I: Fluid Mechanics*, Wiley, New York, 1977.
16. H. Saïto and L. E. Scriven, 'Study of coating flow by the finite element method', *J. Comp. Physics*, **42,** 53 (1981).
17. R. E. Nickell, R. I. Tanner and B. Caswell, 'The solution of viscous incompressible jet and free surface flows using finite element methods', *J. Fluid Mech.*, **65,** 189 (1974).
18. W. J. Silliman and L. E. Scriven, 'Separating flow near a static contact line: slip at a wall and shape of a free surface', *J. Comp. Physics*, **34,** 287 (1980).
19. O. C. Zienkiewicz and P. N. Godbole, 'Viscous incompressible flow with special reference to non-Newtonian (plastic) fluids' in R. H. Gallager (ed), *Finite Element in Fluids*, Vol. 1, p. 25, Wiley, 1975.
20. C. Cuvelier, 'A free boundary problem in hydrodynamic lubrication including surface tension', *Proc. VIth. Inst. Conf. on Num. Meth. in Fluid Dynamics*, Tbilissi (USSR), 39 (1978).
21. C. Y. Lee and J. A. Tallmadge, 'Description of meniscus profile in free coating II. Analytical expressions', *AIChE J.*, **19,** 403.
22. P. Tanguy, L. Choplin, M. Fortin and M. Robichaud, 'Dip coating with second-order fluids', submitted to *J. Non-Newt. Fluid Mech.*